Available online at www.sciencedirect.com
ScienceDirect
Journal of Controlled Release 122 (2007) 261–268
journal of controlled release
www.elsevier.com/locate/jconrel

Paclitaxel distribution in poly(ethylene glycol)/poly(lactide-co-glycolic acid) blends and its release visualized by coherent anti-Stokes Raman scattering microscopy

Eunah Kang [a], Joshua Robinson [c], Kinam Park [a,b,*], Ji-Xin Cheng [a,c,*]

[a] *Weldon School of Biomedical Engineering, Purdue University, West Lafayette, Indiana, United States*
[b] *Department of Pharmaceutics, Purdue University, West Lafayette, Indiana, United States*
[c] *Department of Chemistry, Purdue University, West Lafayette, Indiana, United States*

Received 16 February 2007; accepted 8 May 2007
Available online 17 May 2007

Abstract

Mechanisms underlying the release of paclitaxel (PTX) from poly(ethylene glycol)/poly(lactic-co-glycolic acid) (PEG/PLGA) blends were investigated by coherent anti-Stokes Raman scattering (CARS) microscopy. PLGA, PEG, and PTX were selectively imaged by using the resonant CARS signal from the CH_3, CH_2, and aromatic CH stretch vibrations, respectively. Phase segregation was observed in PLGA films containing 10 to 40 wt.% PEG in the absence of PTX loading. The PEG phase existed in the form of crystalline fibers in the (8:2, weight ratio) and (7:3) PLGA/PEG films. CARS observation indicated that PTX preferentially partitioned into the PEG domains in the (9:1) and (8:2) PLGA/PTX films, but exhibited a uniform mixing with both PLGA and PEG in the (7:3) PLGA/PEG film. The solid dispersion of PTX into PEG domains was attributed to a strong interaction between PTX and PEG, supported by the disappearance of PEG crystallization in the PTX-loaded PLGA/PEG film evidenced through X-ray diffraction analysis. PTX release was induced by exposing the film to an aqueous solution and monitored in real time by CARS and two-photon fluorescence microscopy. Fast dissolution of both PEG and PTX was observed at the film surface. Upon infiltration of water into the film, the PEG domains were rearranged into ring structures enriched by both PTX and PEG. The CARS data provided visual evidence explaining the accelerated burst release followed by more sustained release of PTX from the PLGA/PEG films as measured by HPLC.
© 2007 Elsevier B.V. All rights reserved.

Keywords: PLGA; Paclitaxel; PEG; CARS microscopy; Molecular imaging

1. Introduction

PTX has been administered with a great success in the treatment of in-stent restenosis [1–3]. Being biodegradable and biocompatible, PLGA is widely used for delivery of PTX and other drugs coated on stents [1,4–6]. To compromise the brittle mechanical properties of PLGA, PEG of low glass transition temperature was often added as a plastizer to the PLGA matrix [6,7]. The PEG addition also resulted in accelerated or decelerated drug release in a controlled manner [7–10]. For instance, adding 2% PEG to PLGA microparticles increased the *in vitro* release rate of PTX, while higher portion of PEG slowed down the PTX release [10].

In most studies, the drug release profiles were characterized by chemical analysis methods such as HPLC. While convenient and widely used, such chemical analysis does not tell the redistribution of drugs inside a delivery system that may occur during the release process. As a consequence, although the two basic pathways (diffusion and degradation) for drug release from a polymer matrix have been established [11], the detailed mechanisms which may be related to phase segregation according to polymer-drug interactions remain elusive.

Molecular imaging recently emerged as a new tool for drug release studies. FT-IR imaging of PEG dissolution in an aqueous environment has been implemented to investigate the drug release mechanism [12–15]. While this method provides

* Corresponding authors. Weldon School of Biomedical Engineering, Purdue University, West Lafayette, Indiana, United States. Tel.: +1 765 494 4335; fax: +1 765 496 1912.
E-mail addresses: kpark@purdue.edu (K. Park), jcheng@purdue.edu (J.-X. Cheng).

0168-3659/$ - see front matter © 2007 Elsevier B.V. All rights reserved.
doi:10.1016/j.jconrel.2007.05.007

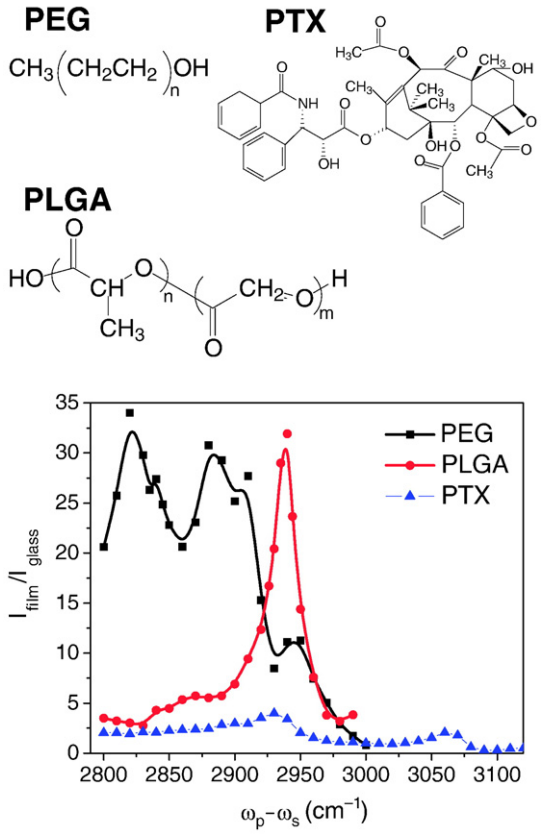

Fig. 1. CARS spectra of PEG, PLGA, and PTX in the CH vibration region. The molecular structures are shown above the spectra. The two peaks at 2820 cm^{-1} and 2890 cm^{-1} arise from the symmetric and asymmetric CH_2 stretch vibration in PEG. The peak at 2940 cm^{-1} arises from the CH_3 stretch vibration in PLGA. The 3060 cm^{-1} peak arises from the aromatic CH stretch vibration in PTX.

chemical selectivity, the long excitation wavelength used in FT-IR microscopy offers the spatial resolution of several to tens micrometer, which does not allow the visualization of 3D distribution of drug molecules in thin polymer films or microparticles. Raman microscopy [16–18] provides better spatial resolution by using a shorter excitation wavelength, but the weak Raman scattering necessitates a long image acquisition time from minutes to hours. A recently developed nonlinear optical imaging technique that is based on coherent anti-Stokes Raman scattering (CARS) circumvents these difficulties. In CARS microscopy [19], a pump laser beam at frequency ω_p and a Stokes laser beam at frequency ω_s are collinearly overlapped and tightly focused into a sample to generate a signal at the anti-Stokes frequency $\omega_{as}=\omega_p-\omega_s+\omega_p$. CARS microscopy offers the following advantages. First, the CARS signal can be significantly enhanced when $\omega_p-\omega_s$ is tuned to a Raman-active molecular vibration, which provides the molecular selectivity. Second, the coherent addition produces a large CARS signal, which allows high-speed imaging of dynamic systems. Third, the nonlinear dependence of signal generation on the excitation laser intensity ensures that the CARS signal is only produced at the focal center, providing 3D spatial resolution. Recently, Kang et al. demonstrated CARS imaging of PTX dispersion and coagulation in films of different polymers [20]. In this work, CARS microscopy was used to map the distribution of PTX in spray-coated films of PLGA/PEG blend and to monitor the reorganization of PEG and PTX during the release process. The sample used in our study mimics the film coated on a drug-eluting stent. The CARS imaging results interpret the PTX release profiles measured by HPLC.

2. Materials and methods

2.1. Chemicals

Poly(ethylene glycol) (PEG, MW 2000) was obtained from Sigma-Aldrich (Berkeley, CA). Poly(lactic-co-glycolic acid) (PLGA, equimolar lactic and glycolic acids, nominal inherent viscosity=0.59 dl/g, MW 4.4×10^4) was purchased from Birmingham Polymers, Inc. (Pelham, AL). Paclitaxel (PTX, MW 854) was kindly supplied by Samyang, Ltd. (Seoul, Korea).

2.2. Film preparation

Solutions of 1 wt.% PLGA/PEG/PTX with various ratios were prepared in the co-solvent composed of (4:1) tetrahydrofuran/toluene. The solution was deposited on a cover glass by spray coating. Micro mists were sprayed to the cover glass through an air brush connected with an air compressor. The

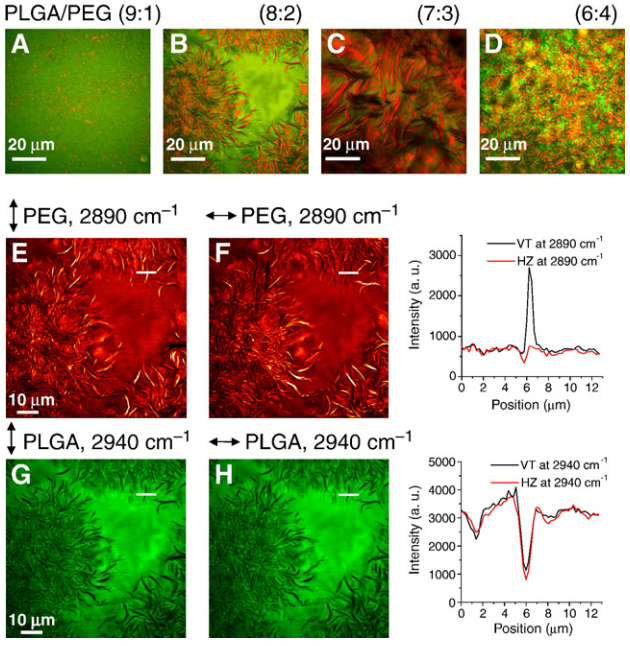

Fig. 2. Phase segregation and crystallization in PEG/PLGA films visualized by CARS microscopy. (A–D) CARS images of the (A) PEG10%/PLGA90%, (B) PEG20%/PLGA20%, (C) PEG30%/PLGA70%, (D) PEG40%/PLGA60% films. The red and green colors represent the CARS intensities for PEG and PLGA, acquired at 2890 cm^{-1} and 2940 cm^{-1}, respectively. (E–H) Polarization analysis of the PEG20%/PLGA80% film. (E) Image taken at 2890 cm^{-1} with vertical excitation polarization. (F) Image taken at 2890 cm^{-1} with horizontal polarization. (G) Image taken at 2940 cm^{-1} with vertical polarization. (H) Image taken at 2940 cm^{-1} with horizontal polarization. The CARS intensities along the white lines in the images are shown on the right side. VT: vertical. HZ: horizontal. An autumn color scheme was used to signify the CARS intensity dependence on excitation polarization in (E) and (F).

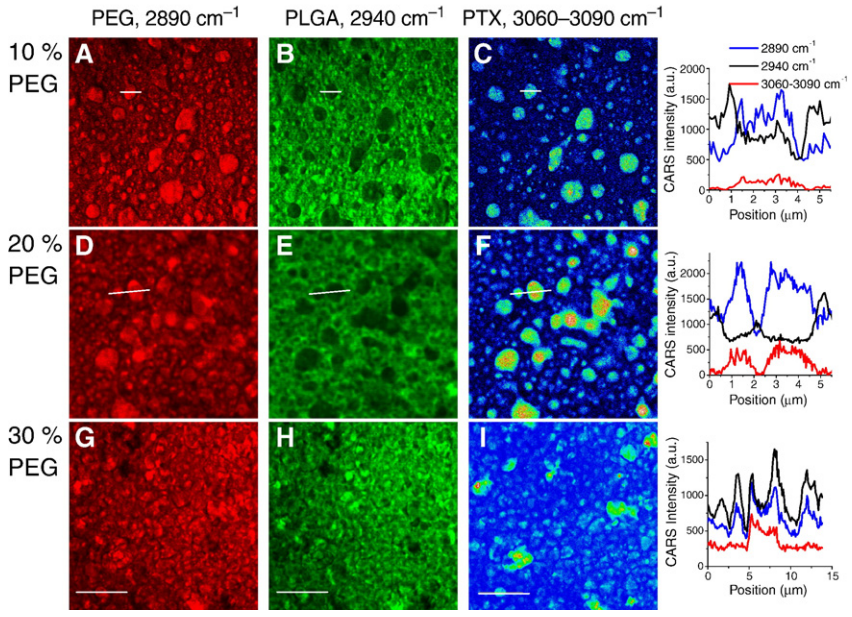

Fig. 3. Distribution of paclitaxel (15% of the total weight) in films composed of (a) PEG10%/PLGA90%, (b) PEG20%/PLGA20%, (c) PEG30%/PLGA70%. Images in the first column and the second column were taken at 2890 cm^{-1} and 2940 cm^{-1}, respectively. Images in the third column were constructed from the signal difference between 3060 cm^{-1} and 3090 cm^{-1}. The forth column presents the CARS intensities along the white lines in the images.

formed films were dried under the vacuum for 24 h at 25 °C to completely remove the solvent. The film thickness was around 20 μm.

2.3. CARS microscopy

Details about our laser-scanning CARS microscope were described elsewhere [21]. Briefly, two tightly synchronized Ti: sapphire lasers (Mira900, Coherent Inc.) were used to generate the 2.5-ps pump and Stokes beams, respectively. The two parallel-polarized laser beams were collinearly combined and directed into a laser scanning microscope (Olympus America Inc, FV300/IX70). A Pockels cell was used to reduce the pulse repetition rate from 76 MHz to 1.3 MHz. A water immersion objective with a numerical aperture of 1.2 was used to focus the laser beams into the polymer film sample. The CARS signal from the sample was detected in the forward direction by a photomultiplier tube (Hamamatsu, R3896). The acquisition speed was 1.12 s/frame. The pump and Stokes power at the sample was 1.0 and 0.4 mW, respectively. All the imaging experiments were conducted at the optics lab temperature of 22 °C. The CARS spectra of PLGA, PEG, and PTX films were recorded by manually tuning the Stokes laser wavelength. The CARS signal from the sample was normalized by the nonresonant CARS signal from the cover glass at each wavelength to remove the intensity fluctuation induced by the variation in laser power and detection efficiency.

2.4. HPLC analysis of PTX release profile

A cover glass coated with a PLGA/PEG/PTX film was attached to the frame of a bottom-glass petri dish. PTX was released at 25 °C in a phosphate-buffered saline (PBS, pH 7.4). The release medium in the chamber was sampled and replaced with a fresh medium at timed intervals. The released PTX in the medium was analyzed using HPLC (Agilent 1100 series) at 37 °C. The PTX was measured by absorption at 227 nm. The samples were run at a flow rate of 1.0 mL/min. Acetonitrile (ACN) and water with ratio of 40:60 were used as the mobile phase.

2.5. X-Ray diffraction analysis

X-ray diffraction (XRD) analysis was performed with a Siemen's X-ray diffractometer equipped with Cu K_α radiation. Film samples of pure PEG, PLGA/PEG, and PLGA/PEG/PTX were analyzed in the range of 6 to 40° with an angular resolution of 0.04°. The films were prepared by spray coating on the quartz

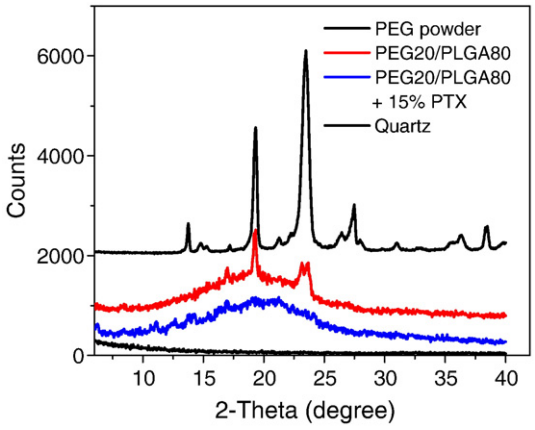

Fig. 4. X-ray diffraction analysis of the PTX power and various polymer films. The disappearance of the sharp peaks in the PEG20/PLGA80/15%PTX film indicates a strong interaction between PEG and PTX.

holder (Gem Dugout, PA) which has a low X-ray background. The exposure time for each measurement was about 15 min.

3. Results

3.1. CARS spectra of PEG, PLGA, and PTX

CARS spectra of PEG, PLGA, or PTX in the CH vibration region (Fig. 1) were recorded to determine the suitable Raman bands for selective imaging of these molecules in the blend film. For the PEG film, two broad peaks were observed around 2890 cm^{-1} and 2820 cm^{-1}, corresponding to the asymmetric and symmetric CH_2 stretch vibration, respectively. For PLGA which is abundant in CH_3 groups, a pronounced peak arising from the symmetric CH_3 stretching appeared at 2940 cm^{-1}. For PTX, we observed a peak at 3060 cm^{-1} and a dip at 3090 cm^{-1} that are characteristic of the CARS band of aromatic CH stretch vibration.

The 2940 cm^{-1} peak allows the selective imaging of PLGA. The 2820 cm^{-1} and 2890 cm^{-1} peaks give similar contrast in CARS images of blend films. To reduce the laser wavelength tuning range, the 2890 cm^{-1} peak was chosen for imaging PEG. The CARS signal from PTX is relatively weak. In order to completely remove the nonresonant background contributed by PEG and PLGA, the CARS intensity at 3060 cm^{-1} (peak) was subtracted by that from 3090 cm^{-1} (dip) and the difference signal was used to map the distribution of PTX.

3.2. Phase segregation and crystallization in PLGA/PEG blend

CARS microscopy was first used to image the PLGA/PEG films prepared without PTX loading. The weight percentage of PEG in the films varied from 0 to 40%. The laser beams were focused at the mid-depth of the films. The pure PLGA film exhibited a uniform CARS intensity distribution (data not shown). The CARS images for films containing 10 to 40% PEG are shown in Fig. 2, with the red and green colors representing the contrast for PEG and PLGA, respectively. Phase segregation was observed in the (9:1) PLGA/PEG film, with the PEG enriched phase separated as small islands in the percolating PLGA matrix (Fig. 2A). In the (8:2) PLGA/PEG film, the PEG enriched phase formed fibers in the continuous PLGA phase (Fig. 2B). With the PEG percentage increased to 30%, the PEG fibers were observed all over the film, whereas the area enriched in PLGA was reduced (Fig. 2C). Phase separation was also observed in the (6:4) PEG/PLGA film but with few fiber-like structures (Fig. 2D).

Crystallization of polyethylene oxide in thin films has been reported [22]. Herein, the dependence of the CARS signal on excitation polarization was analyzed to determine the existence of PEG crystallization in the blend film. For the (8:2) PLGA/PEG film, the CARS intensity at 2890 cm^{-1} from the fiber shows a clear dependence on laser polarization. An enhanced contrast was observed when the incident beams were polarized along the fiber (Fig. 2 E, F). Because the CARS signal from symmetric CH_2 stretch is maximized when the excitation polarization is parallel with the dipole of the CH_2 group [23], our result indicates that the symmetry axis of most CH_2 groups is aligned along the fiber. The polarization dependence demonstrates that PEG in the fiber exists in a crystalline form. Meanwhile, the CARS intensity at 2940 cm^{-1} was not reliant on the laser polarization (Fig. 2G, H), consistent with the amorphous nature of PLGA. In films containing 10% and 40% PEG, no polarization dependence was observed for either PEG or PLGA.

3.3. PTX distribution in PLGA/PEG films

PTX-loaded films were prepared by adding PTX (15 wt.% of the total blend weight) to the solution of (8:2) PLGA/PEG blend followed by spray coating. The distribution of PTX was mapped by the CARS signal from aromatic CH vibration. The PTX exhibited a uniform distribution in a PLGA film as shown in our earlier work [20]. Phase segregation was clearly observed in films containing 10% PEG (Fig. 3A, B). The CARS contrast from PTX (Fig. 3C) showed the same spatial pattern as that from PEG, indicating that PTX was localized in the PEG phase (Fig. 3A). Moreover, PTX was uniformly distributed (i.e., no coagulation) in the isolated PEG domains. As the PEG content increased to 20%, PTX was still preferentially partitioned into the confined PEG domains (Fig. 3D–F). Notably, no fiber structure was observed from the PEG phase and no polarization

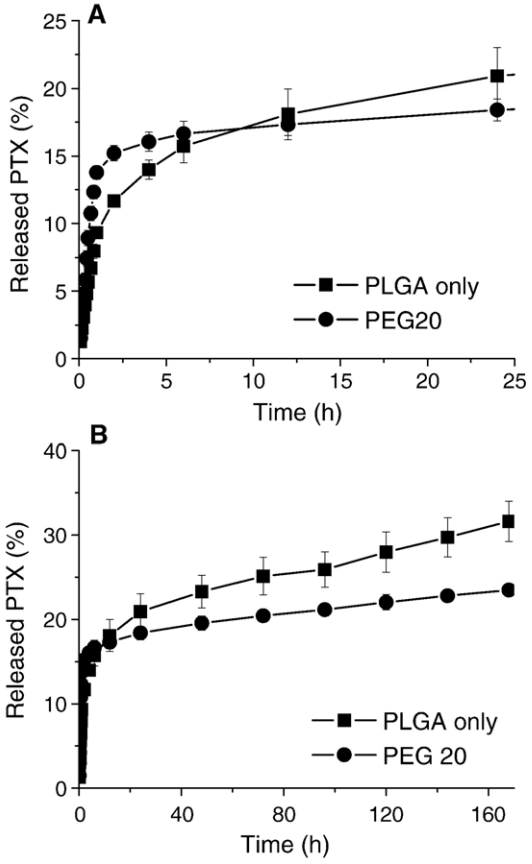

Fig. 5. Release of PTX from the PEG20%/PLGA80% film measured by HPLC. Phosphate-buffered saline (PBS) was used as the releasing medium. (A) Short term release in 24 h. (B) Long term release in 200 h.

dependence of the CARS signal was identified, indicating that PEG crystallization could be prevented by the interaction between PTX and PEG. For the film containing 30% PEG, PLGA, PEG, and PTX exhibited the same spatial distribution pattern (Fig. 3G–I), indicating a better miscibility between the polymers and drug at this composition. The distribution of PLGA, PEG, and PTX was quantified with line analysis shown in the forth column of Fig. 3. For films containing 10% and 20% PEG, the intensity profiles showed the same spatial pattern for PEG and PTX and clear segregation between PEG and PLGA phase.

To provide independent evidence for the observed spatial colocalization of highly hydrophobic PTX with hydrophilic PEG, we recorded the XRD spectra of PEG powder and different films. The results are shown in Fig. 4. The crystalline PEG powder showed intensive X-ray pattern, in coincidence with previous studies [24–26]. The XRD spectrum of the (8:2) PLGA/PEG film displayed two peaks at 19.3° and 23.5° which were located at the same position with the PEG powder, and a broad amorphous band between 10 to 30° which resulted from the amorphous PLGA phase. The sharp XRD peaks indicate the crystallization of PEG in the (8:2) PLGA/PEG film, in consistence with the crystalline fibers observed in the CARS images. A change in the XRD pattern was observed in PTX-loaded (8:2) PLGA/PEG film: the sharp peaks at 19.3° and 23.5° disappeared and only the broad amorphous band over 10 to 30° was observed. This result suggested that PEG strongly interacts with PTX in the film. Taken together, the CARS and XRD data demonstrated that PTX was dispersed in the solid PEG phase. Its effect on PTX release is studied below.

3.4. Study of PTX release by HPLC and CARS microscopy

The amount of PTX released from the (8:2) PLGA/PEG blend film and the PLGA film was analyzed by HPLC, using PBS as the releasing medium. The short-term (24 h) and long-term (200 h) release profiles were depicted in Fig. 5A and B, respectively. Compared with PTX release from the PLGA matrix, addition of 20% PEG accelerated the burst release of PTX in the first 8 h (Fig. 5A). After the initial stage, the accumulated PTX release rate from the PLGA/PEG film became slower than that from the PLGA film (Fig. 5B).

To directly monitor the release of PTX that was initially distributed in the PEG phase, we carried out time-lapse CARS imaging of a (8:2) PLGA/PEG film loaded with 15 wt.% PTX and placed in a releasing medium. The spectral overlap between the OH stretch vibration in water and the aromatic CH vibration in PTX was avoided by using deuterium water (D_2O) as the releasing medium. The PEG and PTX distribution before and after 40 min release are shown in Fig. 6. Initially, PEG and PTX were colocalized into islands at different depths of the sample. After the 40 min release, pores were observed on the film surface due to the dissolution of PEG. Meanwhile, the CARS signal from PTX became weaker, indicative of PTX release from the film surface (the first row of Fig. 6). After the 40 min release, pores were also observed inside the film and ring

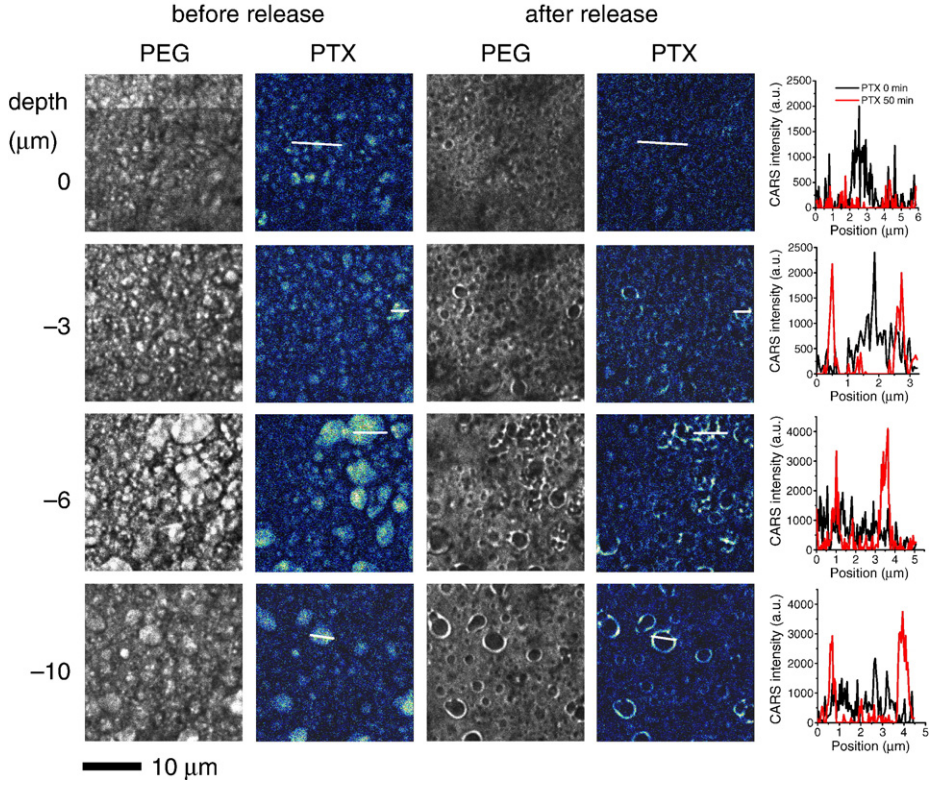

Fig. 6. PTX redistribution before and after the 40 min release process. The first row represents CARS images taken at the film surface. The second to fourth rows represent CARS images taken at 3, 6, 10 μm deep into the film. PEG was visualized by the CARS contrast at 2890 cm^{-1}. PTX was visualized by the CARS signal difference between 3060 cm^{-1} and 3090 cm^{-1}. The fifth column presents the CARS intensities along the white lines in the second and fourth columns.

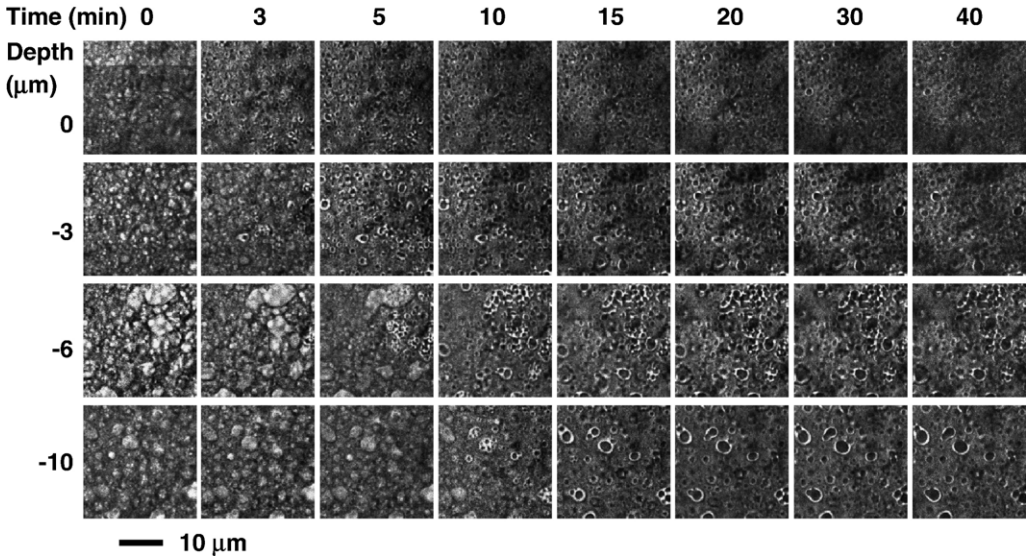

Fig. 7. Temporally and spatially resolved CARS images of initial PEG dissolution in the PEG20/PLGA80/15%PTX film. The columns were arrayed as the time lapse and the rows were arrayed as the depth into the film. CARS images were acquired at 2890 cm^{-1}. The acquisition time for each image was 1.12 s.

structures were formed around the pores. It is interesting that the ring structures showed a bright contrast with the laser wavelengths tuned to the aliphatic CH_2 vibration for PEG and the aromatic CH vibration for PTX (see the intensity profiles in the last column of Fig. 6). The integrated CARS intensity of PTX from the ring structure was roughly the same as that from the isolated phase before the release. This result indicates that PTX was largely redistributed at the interface of PLGA and PEG phases and maintained inside the film.

Time- and depth- resolved CARS images of PEG dissolution are shown in Fig. 7. At the film surface, pores and ring structures appeared in 3 min after placing the film under deuterium water. The CARS signal from the rings gradually reduced with the dissolution of PEG in the aqueous phase. The appearance of pores was delayed as a function of depth. At 10 μm under the surface, the rings appeared after the film was exposed in D_2O for 10 min. It is noteworthy that the ring structures remained the same in the next 30 min, indicating that the release of PTX and PEG was effectively reduced by the continuous PLGA matrix in the film.

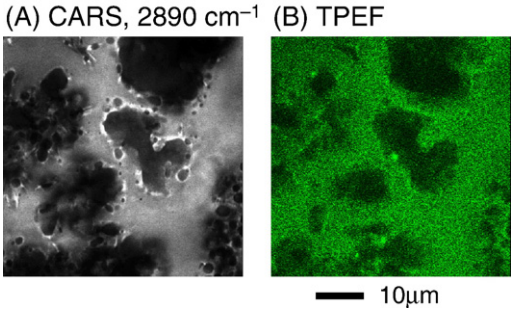

Fig. 8. Imaging of water filtration into the PLGA matrix. (A) CARS image taken at 2890 cm^{-1} at the mid-depth of a film PEG20/PLGA80/15%PTX exposed to D_2O for 30 min. (B) TPEF image of fluorescein (green) taken at the same location. Fluorescein was used as the fluid phase marker.

To have a better understanding of the formation of the ring structures, we further investigated the infiltration of water into the film. Because water has a weak CARS signal, we used fluorescein as a fluid phase marker. Simultaneously acquired CARS images of PEG and two-photon fluorescence images of fluorescein are shown in Fig. 8. After the film was immerged in a fluorescein solution for 30 min, we observed significant fluorescein signals from the PLGA matrix. Upon the contact of the PEG phase with water, it is likely that PEG forms a gel at the PEG/PGLA interface. Conceivably, this PEG dissolution process brings the PTX to the interface, forming a ring structure.

4. Discussion

PEG has been widely used as a drug carrier. The aqueous solubility of a poorly-water soluble drug was shown to be significantly enhanced by up to five orders of magnitude at 80 wt. % of PEG (MW 400) [27,28]. The PTX solubility in PEG dendrimers was even higher than that in PEG (MW 400) solution at the same weight concentration [29,30], probably due to the high local density and conformation arrangement inside the PEG dendrimer. It has been hypothesized that the conformation of PEG chains is rearranged from helix to Zig-Zag which contributes to the high solubility of the drug in an aqueous solution [27]. It has also been speculated that crystalline hydrophobic drug may form hydrogen bonding with PEG in solid solution [31]. Additionally, high miscibility of PEG and hydrophobic drugs including ketoprofen and flurbiprofen was shown in a solid solution state [25,26]. Nevertheless, direct visualization of PTX association with PEG against a hydrophobic polymer has not been reported. In the current study, we directly observed the dispersion of PTX in the PEG domains of phase-segregated PLGA/PEG blend (Fig. 3). The preferential distribution of PTX in the PEG phase over the PLGA phase implied that PEG chain may be entangled with PTX. Such molecular interaction between PEG and PTX was confirmed

by XRD analysis which showed the disappearance of PEG crystallization upon PTX addition (Fig. 4).

Combining the CARS imaging and the HPLC analysis results, we further showed that the solid dispersion of PTX in PEG phase played a critical role in modulating the release of PTX. Due to local PTX partition in the PEG phase, the PEG dissolution accelerated PTX release from the surface at the initial stage. Inside the film, water infiltration redistributes PTX and PEG into ring structures in the continuous PLGA phase. The PLGA matrix conceivably acted as a hydrophobic barrier of PTX diffusion. As a consequence, in the period of 8 to 200 h, we observed a more sustained PTX release from the (8:2) PLGA/PEG film in comparison to the PTX release from the PLGA film.

5. Conclusions

Spatial organization of PLGA, PEG, and PTX in spray-coated blend films was characterized by CARS microscopy. Without PTX loading, PLGA and PEG were segregated into two phases. PEG formed crystalline fibers inside the amorphous PLGA matrix in the (8:2) and (7:3) PLGA/PEG films. With the addition of 15% PTX to the (8:2) PLGA/PEG film, the PEG crystallization disappeared as evidenced by XRD analysis. Importantly, PTX was partitioned into the PEG phase, which affected the release profiles of PTX. Compared with PTX release from pure PLGA matrix, addition of PEG accelerated the burst release of PTX through dissolution of PEG and PTX at the film surface. The PTX inside the films was reorganized into ring structures upon water infiltration and its release was retarded by the continuous PLGA matrix. As a result, a sustained release in 8 to 200 h was observed. Our results show that drug release from a polymer matrix is closely related with its distribution. With the capability of visualizing drug and polymer molecules with 3D spatial resolution and no need for labeling, CARS microscopy holds a great potential in drug delivery formulation research.

Acknowledgements

This work is supported by NIH through grant HL78715. The authors thank Alan P. Kennedy and Haifeng Wang for help in the experiments.

References

[1] A. Colombo, J. Drzewiecki, A. Banning, E. Grube, K. Hauptmann, S. Silber, D. Dudek, S. Fort, F. Schiele, K. Zmudka, G. Guagliumi, M.E. Russell, Randomized study to assess the effectiveness of slow- and moderate-release polymer-based paclitaxel-eluting stents for coronary artery lesions, Circulation 108 (2003) 788–794.

[2] R. Wessely, A. Schomig, A. Kastrati, Sirolimus and paclitaxel on polymer-based drug-eluting stents: similar but different, J. Am. Coll. Cardiol. 47 (2006) 708–714.

[3] B. Scheller, C. Hehrlein, W. Bocksch, W. Rutsch, D. Haghi, U. Dietz, M. Bohm, U. Speck, Treatment of coronary in-stent restenosis with a paclitaxel-coated balloon catheter, N. Engl. J. Med. 355 (2006) 2113–2124.

[4] C.J. Pan, J.J. Tang, Y.J. Weng, J. Wang, N. Huang, Preparation, characterization and anticoagulation of curcumin-eluting controlled biodegradable coating stents, J. Control. Release 116 (2006) 42–49.

[5] S.S. Venkatraman, L.P. Tan, J.F.D. Joso, Y.C.F. Boey, X.T. Wang, Biodegradable stents with elastic memory, Biomaterials 27 (2006) 1573–1578.

[6] X.T. Wang, S.S. Venkatraman, F.Y.C. Boey, J.S.C. Loo, L.P. Tan, Controlled release of sirolimus from a multilayered PLGA stent matrix, Biomaterials 27 (2006) 5588–5595.

[7] L.P. Tan, S.S. Venkatraman, P.F. Sung, X.T. Wang, Effect of plasticization on heparin release from biodegradable matrices, Int. J. Pharm. 283 (2004) 89–96.

[8] R.L. Cleek, K.C. Ting, S.G. Eskin, A.G. Mikos, Microparticles of poly (DL-lactic-co-glycolic acid)/poly(ethylene glycol) blends for controlled drug delivery, J. Control. Release 48 (1997) 259–268.

[9] E.L. Hedberg, C.K. Shih, L.A. Solchaga, A.I. Caplan, A.G. Mikos, Controlled release of hyaluronan oligomers from biodegradable polymeric microparticle carriers, J. Control. Release 100 (2004) 257–266.

[10] L. Mu, M.M. Teo, H.Z. Ning, C.S. Tan, S.S. Feng, Novel powder formulations for controlled delivery of poorly soluble anticancer drug: application and investigation of TPGS and PEG in spray-dried particulate system, J. Control. Release 103 (2005) 565–575.

[11] R. Langer, New methods of drug delivery, Science 249 (1990) 1527–1533.

[12] C.A. Coutts-Lendon, N.A. Wright, E.V. Mieso, J.L. Koenig, The use of FT-IR imaging as an analytical tool for the characterization of drug delivery systems, J. Control. Release 93 (2003) 223–248.

[13] J. van der Weerd, S.G. Kazarian, Combined approach of FTIR imaging and conventional dissolution tests applied to drug release, J. Control. Release 98 (2004) 295–305.

[14] K.L.A. Chan, S.G. Kazarian, FTIR spectroscopic imaging of dissolution of a solid dispersion of nifedipine in poly(ethylene glycol), Mol. Pharmacol. 1 (2004) 331–335.

[15] I.W. Levin, R. Bhargava, Fourier transform infrared vibrational spectroscopic imaging: integrating microscopy and molecular recognition, Annu. Rev. Phys. Chem. 56 (2005) 429–474.

[16] G. Turrell and J. Corset. Academic Press Inc., San Diego 1996.

[17] J. Ling, S.D. Weitman, M.A. Miller, R.V. Moore, A.C. Bovik, Direct Raman imaging techniques for study of subcellular distribution of a drug, Appl. Opt. 41 (2002) 6006–6017.

[18] N. Uzunbajakava, A. Lenferink, Y. Kraan, E. Volokhina, G. Vrensen, J. Greve, C. Otto, Nonresonant confocal Raman imaging of DNA and protein distribution in apoptotic cells, Biophys. J. 84 (2003) 3968–3981.

[19] J.X. Cheng, X.S. Xie, Coherent anti-Stokes Raman scattering microscopy: instrumentation, theory, and applications, J. Phys. Chem., B 108 (2004) 827–840.

[20] E. Kang, H. Wang, I.K. Kwon, J. Robinson, K. Park, J.X. Cheng, In situ visualization of paclitaxel distribution and release by coherent anti-Stokes Raman scattering microscopy, Anal. Chem. 78 (2006) 8036–8043.

[21] H. Wang, Y. Fu, P. Zickmund, R. Shi, J.X. Cheng, Coherent anti-Stokes Raman scattering imaging of axonal myelin in live spinal tissues, Biophys. J. 89 (2005) 581–591.

[22] H. Schonherr, C.W. Frank, Ultrathin films of poly(ethylene oxides) on oxidized silicon. 2. In situ study of crystallization and melting by hot stage AFM, Macromolecules 36 (2003) 1199–1208.

[23] J.X. Cheng, S. Pautot, D.A. Weitz, X.S. Xie, Ordering of water molecules between phospholipid bilayers visualized by coherent anti-Stokes Raman scattering microscopy, Proc. Natl. Acad. Sci. U. S. A. 100 (2003) 9826–9830.

[24] M. Wulff, M. Alden, D.Q.M. Craig, An investigation into the critical surfactant concentration for solid solubility of hydrophobic drug in different polyethylene glycols, Int. J. Pharm. 142 (1996) 189–198.

[25] T. Ozeki, H. Yuasa, Y. Kanaya, Application of the solid dispersion method to the controlled release of medicine. IX. Difference in the release of flurbiprofen from solid dispersions with poly(ethylene oxide) and hydroxypropylcellulose and the interaction between medicine and polymers, Int. J. Pharm. 155 (1997) 209–217.

[26] D.M. Schachter, J.C. Xiong, G.C. Tirol, Solid state NMR perspective of drug-polymer solid solutions: a model system based on poly(ethylene oxide), Int. J. Pharm. 281 (2004) 89–101.

[27] M.J. Groves, B. Bassett, V. Sheth, The solubility of 17 beta-estradiol in aqueous polyethylene glycol-400, J. Pharm. Pharmacol. 36 (1984) 799–802.

[28] E. Rytting, K.A. Lentz, X.Q. Chen, F. Qian, S. Venkatesh, A quantitative structure-property relationship for predicting drug solubility in PEG 400/water cosolvent systems, Pharm. Res. 21 (2004) 237–244.

[29] T. Ooya, J. Lee, K. Park, Effects of ethylene glycol-based graft, star-shaped, and dendritic polymers on solubilization and controlled release of paclitaxel, J. Control. Release 93 (2003) 121–127.
[30] T. Ooya, J. Lee, K. Park, Hydrotropic dendrimers of generations 4 and 5: synthesis, characterization, and hydrotropic solubilization of paclitaxel, Bioconjug. Chem. 15 (2004) 1221–1229.
[31] S. Chutimaworapan, G.C. Ritthidej, E. Yonemochi, T. Oguchi, K. Yamamoto, Effect of water-soluble carriers on dissolution characteristics of nifedipine solid dispersions, Drug Dev. Ind. Pharm. 26 (2000) 1141–1150.